Westerlies and Asian Monsoons in Middle of China

Subjects: Geography, Physical

Contributor: Bing-Qi Zhu

The westerly circulation and the monsoon circulation are the two major atmospheric circulation systems affecting the middle latitudes of the Northern Hemisphere (NH), which have significant impacts on climate and environmental changes in the middle latitudes. However, until now, people's understanding of the long-term paleoenvironmental changes in the westerly- and monsoon-controlled areas in China's middle latitudes is not uniform, and the phase relationship between the two at different time scales is also controversial, especially the exception to the "dry gets drier, wet gets wetter" paradigm in global warming between the two.

westerlies Asian summer monsoon circulation system interaction different time scale mid-latitude region

1. Changes of the Westerlies and ASM at Different Time Scales and Their Relationships

1.1. Initial Period

The Westerly circulation is a kind of planetary wind system formed by the uneven heating and rotation deflection of the Earth. It has been formed for a long time and its origin is not a controversial issue. Based on the sedimentary records of deep-sea cores in the North Pacific Ocean, Rea et al. [1] speculated that the aeolian material transported by the Westerly circulation in northwest China had already reached a considerable scale at least before 20 Ma B.P. They found a significant increase in the ocean deposition rate around 8 Ma B.P. based on the characteristics of deep-sea sediments in the North Pacific at different periods, indicating a sudden increase in the dust transport strength of the Westerlies.

Regarding the origin of the EASM, Liu et al. [2] inferred the approximate paleoenvironmental conditions of different periods in China since the Cenozoic based on the distribution ranges and temporal changes of geological indicators such as Chinese flora and fauna, salt deposits (potassium, halite, and gypsum), and coal seams in China. They pointed out that, before the Oligocene, the climate in China was mainly controlled by the planetary wind system (i.e., the westerlies) and the climate pattern was basically zonal. They also suggested that the embryonic EAM may have appeared during the Oligocene period (38–24 Ma B.P.) based on the reduction of salt deposits such as gypsum and halite in the southeastern region of China during this period. Further research by Wu F et al. [3] found that, before and after 26 Ma B.P., sediments such as mudstone, shale, and other sediments

indicating a humid environment in the Linxia Basin in western China gradually replaced gypsum, halite, and other evaporites indicating a dry environment. It suggests that the precipitation increased in southeastern China (no longer being a desert environment controlled by the subtropical high climate), and the EAM may have already appeared and reached the temperate zone regions at that time driven by the strongly periodic uplift of the Qinghai–Tibet Plateau, forming an environmental distribution pattern similar to that of today.

Regarding the origin of the SASM, it may appear later than the EASM. Shi and Tang [4] proposed that the SASM may have originated around 22 Ma B.P., based on the characteristics of humification shown by spore pollen records in the Linxia Basin.

According to the large-scale occurrence and distribution of red clay deposits on the Loess Plateau in the late Cenozoic, Cao et al. [5] proposed that the East Asian winter monsoon (EAWM) started from 6–8 Ma, and then existed and evolved to this day. However, according to the existence of continuous dust accumulation in northern China since the early Miocene, Guo [6] pointed out that different circulations carrying large amounts of wind dust and water vapor, respectively, formed an arid inland Asian environment and an Asian-monsoon-dominated environment, and their formation time was at least 22 Ma B.P. ago and has since developed to this day. Therefore, the Siberian high pressure system should have formed earlier than 22 Ma B.P. Subsequently, the EAM system characterized by the combination of winter and summer monsoons was initially established [7]. At the same time, the alternations of the dominant periods of winter and summer monsoons also suggest that the Qinghai–Tibet Plateau had reached a certain height when the EAM system was established, which lead to the aridification in northwest China and Central Asia, as well as the northward shift and strengthening of the Siberian high [8][9].

1.2. From the Middle Pleistocene to the Last Interglacial Period (1200–130 ka B.P.)

The 1.2 Ma B.P. period is considered to be the beginning of the global mid-Pleistocene climate transition (MPT) in the Quaternary. Since then, the fluctuation cycle of global climate and environmental changes has gradually changed from 41 ka to 100 ka. This period is mainly characterized by changes in global climate such as an increase in the amplitude of climate fluctuations [10], a significant increase in global ice volume, a decrease in ocean temperature, and an intensification of land drought [11]. The impact of the MPT on the atmospheric circulation and climate environment in the middle latitudes of China is of great significance and deserves to be emphatically studied.

Through the study of the stable isotopes of carbonates in the sediment cores from the hinterland of the Badanjilin Desert, one of the typical areas of interaction of the westerlies and ASM in the desert zone of northern China, Wang F et al. [12] found that, during the period of 1200–600 ka B.P, the $\delta^{18}O$ and $\delta^{13}C$ values showed a common trend of collaborative increase (**Figure 1**C). This is consistent with the research results of carbonate carbon isotopes in the Cretaceous red layers dominated by the planetary wind system before the Late Oligocene, reflecting intense evaporation under the control of a dry climate. Therefore, it is argued that, during the period of 1200–600 ka B.P., the area was controlled by the Westerly circulation [12]. In addition, the carbonate isotopes of $\delta^{18}O$ and $\delta^{13}C$ from sediment cores in the western Qaidam Basin in the northern Qinghai–Tibet Plateau, which is

dominated by the Westerlies, also showed a synergistic increase trend during the period of 1200–600 ka B.P. (**Figure 1**B), indicating strong evaporation, intensified drought, and the relatively stronger influence of the Westerlies in this region during this period [13]. In addition, the sediment characteristics of loess–paleosol profiles in the Kunlun Mountains and Tianshan Mountains in northwestern China (**Figure 1**A) also reflect the relatively strong Westerly climate during this period [14][15].

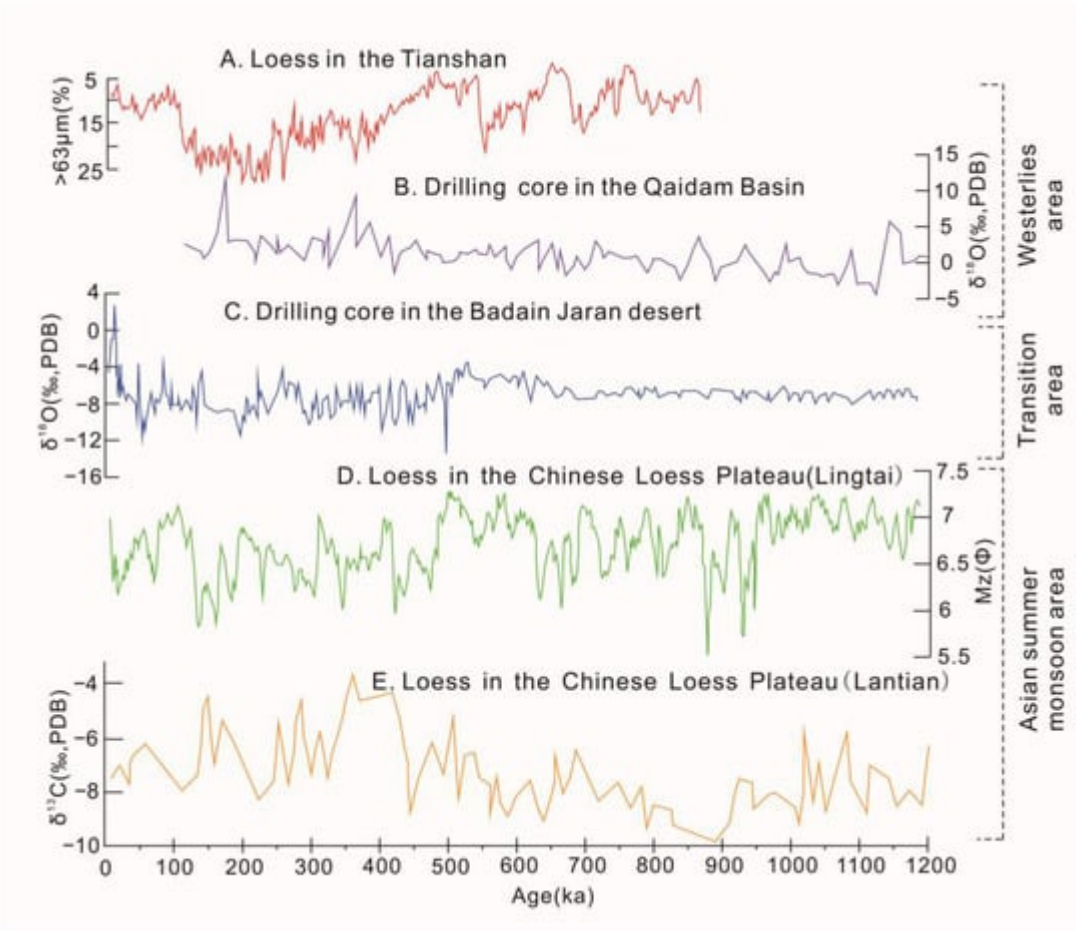

Figure 1. Paleo-sedimentary records from the areas controlled by the Westerly and monsoon circulations since 1200 ka B.P. (**A**) The percentage of grain size > 63 μm in the loess sediment profile on the northern slope of the Tianshan Mountains [15]. (**B**) Variation of $\delta^{18}O$ content in carbonates in the core of the Qaidam Basin [13]. (**C**) Variation of $\delta^{18}O$ content in carbonates in the cores from the hinterland of the Badanjilin Desert [12]. (**D**) Particle size variation of loess sediments in the Lingtai Section of the Loess Plateau [12]. (**E**) Variation of $\delta^{18}O$ content in carbonates of loess sediments in the Lantian Section of the Loess Plateau [16].

However, in the Loess Plateau of China, the ASM climate reflected by paleo-aeolian sedimentary sequences showed the opposite changing characteristics during this period. Variations of grain size and carbonate $\delta^{13}C$ values of the Lingtai and Lantian sections of the Loess Plateau (**Figure 1**D,E) indicate that the sediment particle size is relatively fine and the carbon isotope enrichment degree is weak during this period. The results indicated that the C4 plant biomass in the Loess Plateau was lower, the precipitation in the warm season was less, and the ASM is relatively weak during this period [16][17].

All of the above evidence suggests that, during the period of 1200–600 ka B.P. since the Middle Pleistocene, the Westerly circulation in the middle latitudes of China was relatively strong, while the monsoon circulation was relatively weak. This may be due to the continuous cooling in the high latitudes of the NH during the global MPT and the significant increase in global ice volume, which led to the enhancement of the meridional temperature gradient, the stronger Westerly circulation, the decrease in ocean temperature, and the relative weakening of monsoons [13].

The extensive uplift of the Pamir Plateau and the Qinghai–Tibet Plateau (Kunhuang Movement) that occurred about 600 ka B.P. ago had a profound impact on the changes of the ASM and Westerlies [18], resulting in significant changes in the atmospheric circulations and climatic environment after 600 ka B.P.

In northwest China, where the Westerly climate is dominant, the grain sizes of loess sediments on the northern slopes of the Kunlun Mountains [14] and the Tianshan Mountains [15] were coarsened at around 500 ka B.P., reflecting a significant climatic aridity. This indicates that the substantial uplift of the terrains around the Tarim and Guerbantonggute Basins leads to a decrease of water vapor content brought by atmospheric circulations and a weakening of the Westerly circulation [14][15]. At the same time, the climate in the western Qaidam Basin, which is dominated by the Westerlies, also exhibits similar aridification, because the $\delta^{13}C$ and $\delta^{18}O$ values of the core carbonates from the basin have shown a phased increase since 600 ka B.P. [13], indicating a relative decrease in water vapor content and an intensification of drought compared to the 1200–600 ka B.P. period, that is, a relative weakening of the westerly circulation since 600 ka B.P.

From 450 ka B.P. to 130 ka B.P. in the Last Interglacial period, the climatic environment of the ASM region exhibited relatively large alternating fluctuations corresponding to the glacial–interglacial cycle, and the ASM was exceptionally strong during the interglacial period [19]. During this fluctuation process, the ASM extended northward and westward in the mid-latitude region during the interglacial period, resulting in a relatively strong interaction between the ASM and the Westerly circulation. During the glacial period, the intensity of the ASM is relatively weakened and its impact range is relatively small, so the interaction with the Westerly circulation is also relatively weak.

1.3. Last Interglacial Period (130–70 ka B.P.)

During the Last Interglacial period, the global climate and environmental conditions were similar to the current Holocene, which is reflected in many paleoclimate records.

In the aeolian sediment records of the Loess Plateau in China, climate reconstruction for the Holocene and the early Last Interglacial (Eemian interglacial) periods shows that there was a period of arid climate in the middle of both periods, with the duration of the Holocene drought being 6–5 ka B.P. [20]. The evidence shows that, during the Holocene, the S0 paleosol in the sedimentary profile of the Loess Plateau was interrupted by loess deposition [21], lakes in northern China shrank [22], the amount of terrigenous dust in the seafloor sediments of the North Pacific and the ice cores of Greenland increased [23], and drought events occurred during the Eemian interglacial period

similar to the Holocene [24]. In addition, different climatic records also show that there were relatively humid periods during the Holocene and Eemian interglacial ages, which were in the 5–3 ka B.P. and 124.2–121.3 ka B.P. periods, respectively [24]. The similarity in the patterns of climate change between the Eemian interglacial and Holocene periods revealed by the above cases suggests that research on climate change during the Last Interglacial period may provide some support for predicting the future climate change on Earth [25].

During the Last Interglacial period, records of aeolian sedimentation showed that the atmospheric circulations in the EAM region and the northwest region (westerly region) of China at the middle latitudes were relatively strong (**Figure 2**), with a relatively high precipitation and strong pedogenesis of loess. However, during this period, the intensity of atmospheric circulation and precipitation in different regions may out of phase at the suborbital scale.

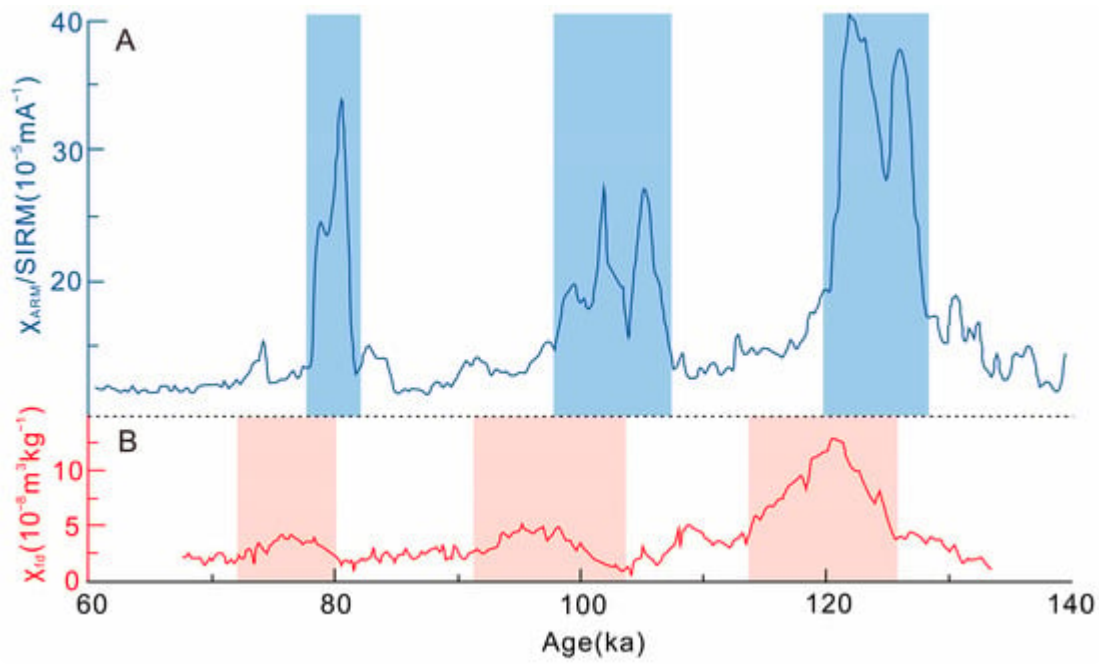

Figure 2. Comparison of the magnetic susceptibility records between the Westerly- and ASM-dominated regions during the Last Interglacial period. (**A**) Changes in magnetic susceptibility recorded in the JZT (Jiuzhoutai) loess sediment profiles on the Loess Plateau of China during the Last Interglacial Period (χARM to SIRM ratio, [26]. (**B**) Changes in frequency magnetic susceptibility in the KS (Kesang) loess sediment profiles in the Yili Basin, northwest China, during the Last Interglacial period [26].

Many paleoclimate records show a lack of co-ordination between the dominant regions of the Westerlies and the ASMs in China in terms of environmental changes during the Last Interglacial period, such as the long-term “out-of-phase” relationship between the moisture evolution patterns of the two regions on the suborbital time scale [27]. For example, in the Loess Plateau dominated by the ASM, the sediment records of loess–paleosol sequences reflect that the moisture content in this area peaked at 78.8, 99.5, 101.5, 103.5, 121.6, and 126.3 ka B.P., indicating that the ASM was relatively strong during these periods and brought a large amount of precipitation to the region [26]. However, in the Yili River Valley of Xinjiang, where the Westerly climate is dominant, the peak values of local moisture reflected by paleoclimatic records such as loess deposits occurred during the periods of 76, 95, 97, 98,

107, and 120.8 ka B.P., respectively [26]. This shows a significant delay of 3–5 ka in the moisture peak values in the Loess Plateau region dominated by the ASM (**Figure 2**), indicating that the moisture evolution patterns of the two during the Last Interglacial period have an out-of-phase relationship on the suborbital time scale.

1.4. Last Glacial Period (70–12 ka B.P.)

In the 1980s, paleoenvironmental records from the Greenland ice cores showed that the predominant characteristic of environmental changes on Earth during the Last Glacial Period (LGP, 70–12 ka B.P.) was the repeated occurrence of abrupt climate changes on millennium time scales [28][29].

During the LGP, 25 D-O cycle events occurred in the North Atlantic region [28], and six significant Heinrich events were recorded by the North Atlantic marine sediments during the coldest interval of the D-O cycles (**Figure 3**a), which contained a large amount of coarse-grained sediments from the land [29].

In the early stage of the LGP (Deep Sea Oxygen Isotope Stage 4, MIS4, 73–61 ka B.P.), more fine-grained sediments (>40 μm) and quartz particles appeared in the loess–paleosol profiles in the Yili region in Central Asia (**Figure 3**b,c). The increase in these materials indicates an enhanced Westerly circulation, leading to coarser dust transport and strong dust storms [30]. While over the Loess Plateau in the ASM region during this period, more coarse particles in the loess profiles (**Figure 3**d) indicated stronger winter monsoon and weaker summer monsoon [31]. However, the low oxygen isotope values of stalagmites from this monsoon region (**Figure 3**e) revealed a strong summer monsoon precipitation [32][33]; that is, a strong summer monsoon occurred.

The changing trends of the Westerlies and monsoons seems to be different during different periods of the LGP. During the MIS4 period, the two regions exhibited a relatively strong Westerly circulation and weak summer monsoon circulation (**Figure 3**). Before MIS3b, the Westerly circulation showed a tendency of decreasing fluctuations, while the summer monsoon circulation showed a trend of increasing fluctuations (**Figure 3**). During the MIS3b-MIS3a period, the fluctuations of the Westerly circulation increased while the fluctuations of the summer monsoon circulation weakened (**Figure 3**).

From these trends, it can be seen that, during the LGP, there may be an inverse correlation between the Westerly and monsoon circulations on the suborbital time scale of the glacial period, but it is not obvious on the whole. Compared with the interglacial period, the ASM during the glacial period was significantly lower [34], and its influence in China was relatively smaller than that during the interglacial period. Thus, its interaction with the Westerly circulation may also be relatively weak. At present, it is still unclear whether there is a complete inverse correlation between the two systems during the glacial period, and more detailed data are needed in the future to explore the interaction between the Westerly and ASM circulations during the glacial period.

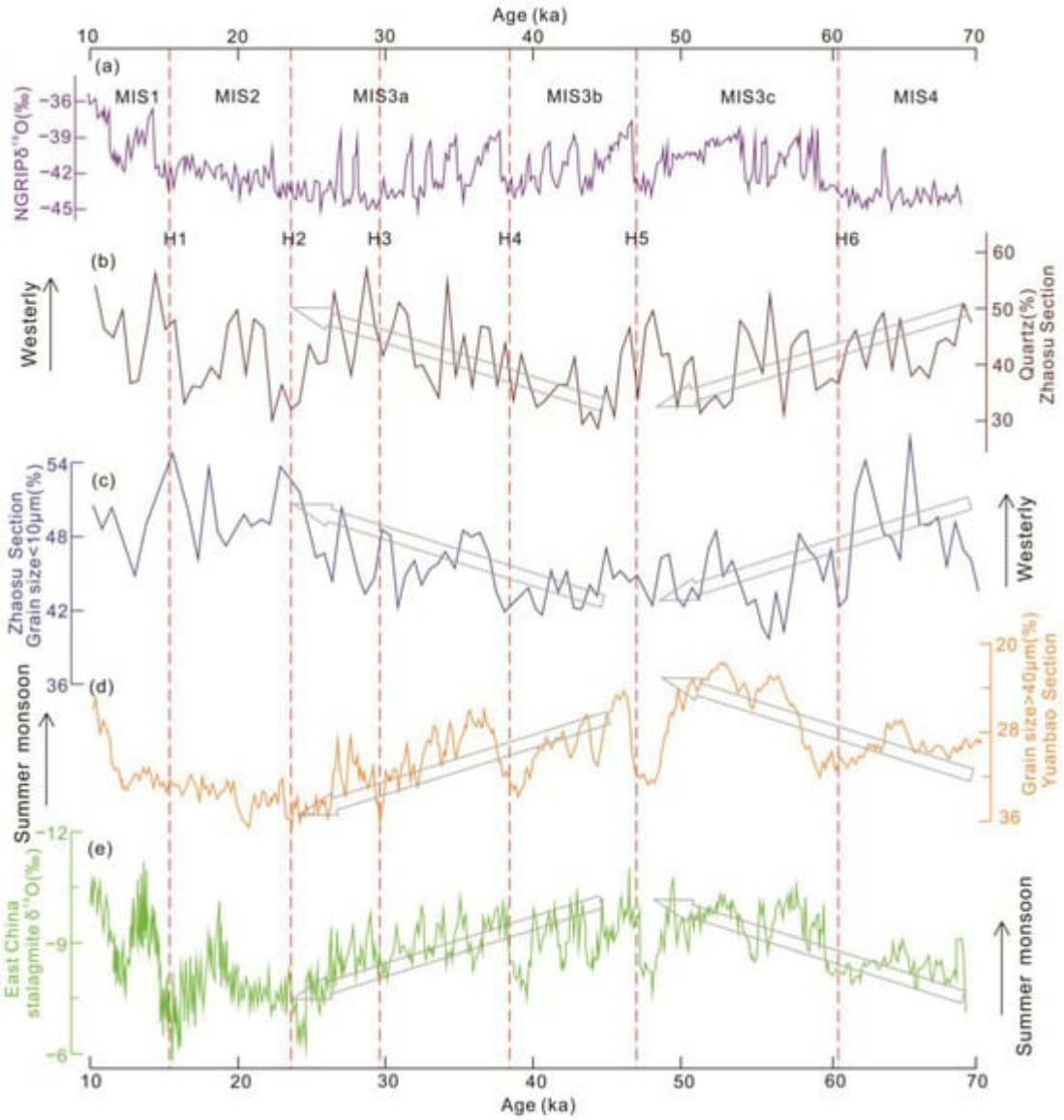

Figure 3. Comparison of records between the Westerly and monsoon regions during the LGP. (**a**) NGRIP Ice Core $\delta^{18}O$ records [35]. (**b**) Changes of quartz content in the Zhaosu section in Yili area dominated by the Westerly climate [30]. (**c**) The percentage variation of sediment grain size < 10 μm in the Zhaosu section [30]. (**d**) The percentage variation of sediment grain size > 40 μm in the Yuanbao section in the monsoon region of South China [31]. (**e**) $\delta^{18}O$ variation of stalagmites in the monsoon region of East China [32]. The arrows indicate the pronounced increase (or decrease) with approximately monotonic trend of the proxies in the corresponding time period.

1.5. The Holocene (12 ka B.P.–1 ka B.P.)

Before the Holocene, the global climate mainly shown a pattern of warm and cold alternation with large fluctuations, while, during the Holocene, it was generally warm with small fluctuations.

For the Westerly-dominated arid region of mid-latitude in China, the climate in this area during the early Holocene (around 11–8 ka B.P.) was drier than it is today (**Figure 4**). During this period, most of the lakes in the region were

in a dry state or had extremely low water levels [36][37], indicating A less precipitation, stronger evaporation, and A weaker Westerly intensity in the region [36][37].

During the middle Holocene (8–4 ka), climate conditions in the arid areas dominated by the Westerlies were relatively humid (**Figure 4**). The ancient records show that the regional precipitation is directly proportional to the intensity of the Westerlies, with an increase in precipitation, and many lakes in the region have the highest water levels in history [38]. This indicates that the strength of the Westerlies has reached its strongest state since the Holocene.

In the late Holocene since 4 ka B.P., the humidity of the climate in the Westerly region decreased (**Figure 4**). The lake water levels in the region were relatively lower, but still higher than in the early Holocene [27]. This indicates that the intensity of the Westerlies in this period had relatively weakened, but the degree of the weakening was small.

Compared with the Westerly region, the climatic conditions in the ASM region during the early Holocene were relatively humid (**Figure 4**). Paleoenvironmental records such as lake sediments in the monsoon region all reflect a higher amount of precipitation [39][40]. The humidification of the monsoon region was mainly related to the relatively strong ASM [41], so the intensity of the ASM in the early Holocene was relatively strong.

From the early Holocene to the middle Holocene, the precipitation in the monsoon region increased relatively, and the degree of humidity and monsoon intensity also gradually increased, reaching the maximum intensity of the Holocene in the middle Holocene [35][42]. This pattern of climate change, which gradually became humid from the early to middle Holocene and reached its strongest level, exhibits different and even opposite characteristics from the pattern of transition from drought to humidity in the Westerly regions during the same period (**Figure 4**).

From the middle to late Holocene, the climate in the monsoon region gradually became arid (**Figure 4**). Compared with the middle Holocene, the precipitation in the monsoon region during this period decreased significantly, and the monsoon intensity showed a continuous weakening trend on the whole [43].

As mentioned above, the Holocene and the Last Interglacial periods were relatively similar in terms of global climate. In fact, in addition to the overall similarity in climatic environment, the intensity variations of the Westerly and ASM circulations in the middle latitudes of Asia during the Holocene, as well as the moisture-changing patterns in their respective influencing areas, were also similar to those in the Last Interglacial period, also showing out-of-phase relationships on the suborbital time scale, as shown in **Figure 4**.

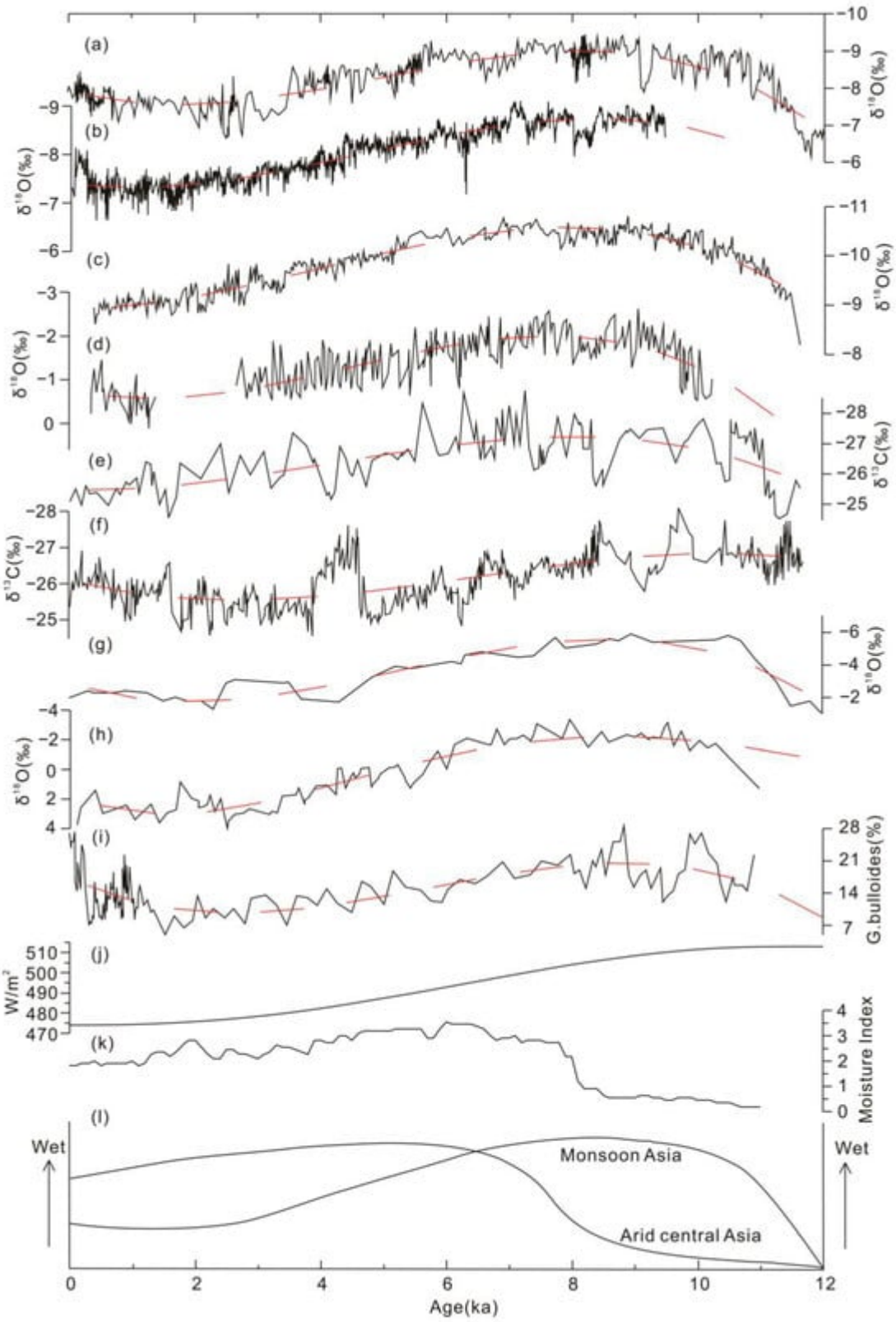

Figure 4. Comparison of paleoenvironmental records between the ASM region and the arid Central Asian region (ACA, the Westerly region) since the Holocene (cited from [38]). (**a**) Dongge Cave D4, China (after [44]); (**b**) Dongge Cave DA, China (after [45]); (**c**) Shanbao Cave SB10-26, China (after [46]); (**d**) Qunf Cave, Oman (after [47]); (**e**) Hongyuan Peat, and (**f**) Hani Peat, China (after [47][48]); (**g**) Siling Lake, China (after [49]); (**h**) Qinghai Lake (after [50]); and (**i**) Arabian Sea (after [51]. All curves in panels (**a**–**i**) show the same direction of moisture change with

increasing moisture upward. The long-term trend for each proxy curve is showed by smooth dashed line. Summer insolation at 30°N ((**j**) after [52]) and synthesized Holocene effective-moisture evolution line (**k**) after [38] are also shown. The out-of-phase relationship of Holocene moisture evolution between monsoon Asia and ACA is illustrated in (**l**).

1.6. Over the Past Thousand Years (1 ka B.P.–Present)

A comparative study of regional paleoenvironmental records from the Westerly region of Central Asia and the monsoon region of East Asia over the past thousand years (1 ka B.P.) has shown that the precipitation in the two regions presents a completely opposite trend during this period [38].

Lake core records from the Westerly-dominated Bosten Lake in Xinjiang show that, during the past 1–0.5 ka B.P. period, the carbonate content of core sediments was relatively high, the coarse particle content was low, and the average particle size was small [53]. This indicates that the humidity of the climate during this period was relatively low, the water vapor content of the atmospheric circulation was less, and the strength of the Westerly circulation was relatively weak. During the period of 0.5–0.1 ka B.P., the regional climate was within the range of the Little Ice Age (LIA), during which the carbonate content in the sediments reached the lowest value, with a higher content of coarse particles and a relatively coarse mean particle size [53]. This indicates that the Westerlies move southward in the NH, the Westerly circulation intensifies and brings more water vapor to the arid areas of Central Asia, resulting in a relatively humid climate. After 0.1 ka B.P., the mean particle size and coarse particle content of lake sediments decreased, while the carbonate content increased again, indicating that the strength of the Westerly circulation weakened again [53]. Therefore, these paleoenvironmental records suggest that the Westerly circulation has exhibited a “weak-strong-weak” changing pattern and trend over the past 1 ka.

2. Regional Impacts of the Westerly and ASM

The middle latitudes of China have a vast area with significant diversity in geological, geographical, topographical, and ecological conditions. Therefore, the climatic environment in different subregions also exhibits significant spatial differences under the influence of the Westerly and ASM circulations.

In the past, scholars often divided China’s climate regionalization into several sub-regions according to the interaction of topographical and meteorological conditions in different regions, which is conducive to identifying and analyzing the influence of different atmospheric circulations on each sub-region [54][55]. Based on previous studies, the mid-latitude region of northern China into three sub-regions is divided. They are the arid region of northwest China located in Central Asia (Westerly region), the humid region of eastern and southern China in East Asia (monsoon region), and the Qinghai–Tibet Plateau region in southwest China (transition/composite/mixed region). Based on the collected paleoclimatic records/indicators (as shown in **Table 1** and **Figure 1**) and modern meteorological data, the degree of influence of different atmospheric circulations in the three regions is dicussed, with a view to more comprehensively understanding the climate and environmental changes that occur in different

mid-latitude regions under the joint effects of the Westerly, ASM, and other atmospheric systems such as the South Asian high (SAH).

2.1. Qinghai–Tibet Plateau Region (QTP, Mixed Zone)

As the highest geographical unit on Earth, the Qinghai–Tibet Plateau (QTP) is highly sensitive to environmental changes in response to global climate change, including permafrost melting, runoff changes, ecological environment changes, and the intensification of natural disasters [56].

The atmospheric circulation system that dominates water vapor transport over the QTP mainly includes two parts, the SASM circulation and the Westerly circulation. According to the different sources of water vapor in the plateau, the academic circle often divides it into two regions, the southern and the northern regions, with a boundary of 32°N [57]. The southern region of the plateau is mainly controlled by the SASM, and the water vapor comes from the slender conveyor belt from the western equatorial Indian Ocean to the Arabian Sea and the Bay of Bengal, which provide about 51.4% of the water vapor for the precipitation on the plateau [58]. The northern region of the plateau is mainly controlled by the low-level Westerlies, and the water vapor comes from Eurasia and the North Atlantic Ocean on the northwest side of the plateau, which provide about 38.9% of the water vapor for the precipitation on the plateau [58].

The QTP has the largest mountain glacier in the world, and its ice core deposits are the best archives to record paleoclimate changes such as precipitation in the past period of the QTP. Research on the paleoenvironmental reconstruction from different ice cores in the northern part of the plateau, such as the Guliya ice core, Dunde ice core, and Puruogangri ice core, has found that the variation trend of precipitation in the northern QTP from west to east had been relatively consistent since the 15th century. That is, the entire northern part of the plateau has experienced a fluctuational increase in precipitation before 1740, a fluctuational decrease in precipitation during 1740–1850, and a fluctuational increase in precipitation after 1850 (**Figure 5**). The consistency of changes in precipitation in this large area indicates that the northern region of the QTP is controlled by an atmospheric circulation system as a whole [59]. Studies of $\delta^{18}O$ in local precipitation have identified that the source of water vapor in the northern plateau is closely related to water vapor transported by the Westerlies [60].

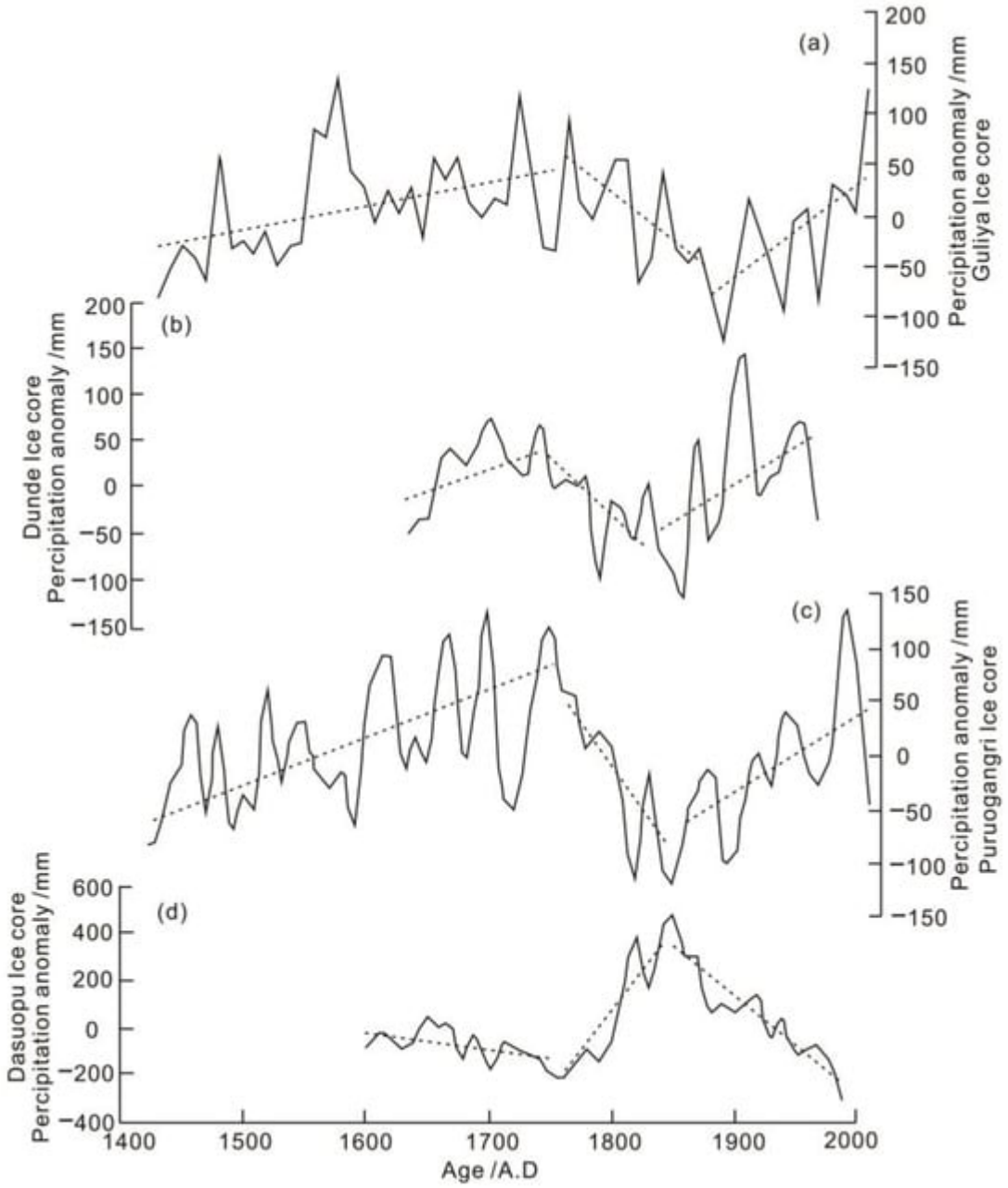

Figure 5. Changes in precipitation over the QTP in recent period as reflected by ice core records (cited from [59]). (**a**) Guiya Ice core. (**b**) Dunde Ice core. (**c**) Puruogangri Ice core. (**d**) Dasuopu Ice core.

However, compared with the precipitation records in the northern part of the QTP, the precipitation records reflected by the Dasopu ice core in the southern part of the QTP show the opposite characteristics [60]. The precipitation in the southern plateau was fluctuationally decreased before 1740, fluctuationally increased during 1740–1850, and then fluctuationally decreased after 1850 [60]. The $\delta^{18}O$ records of regional precipitation show that the source of water vapor in the southern plateau is closely related to water vapor transported by the Indian summer monsoon (ISM) [60].

The QTP is a typical region where the Westerly and monsoon circulations interact, and the coupling state of the two is mainly affected by the variation of monsoon intensity. When the intensity of monsoon is relatively strong, the

position of the Westerlies is northward and the intensity of the Westerlies is relatively weak [61]. On the contrary, when the monsoon intensity is weak, the position of the Westerlies is southward and the intensity of the westerlies is relatively strong [61].

2.2. Northwest China (Westerly Zone)

Compared with the humid environment under the control of monsoon circulation, the climate in northwest China under the control of Westerly circulation is relatively arid due to its long distance from the source areas of water vapor such as the Atlantic Ocean. The main area of the vast mid-latitude desert zone in the NH is mainly distributed in these regions. Therefore, in terms of environmental change, the climate humidification in northwest China is the focus of attention.

Currently, multiple studies have shown that the climate in northwest China has an overall trend of warming and wetting since the mid-20th century. During this period, the lake area in northwest China generally expanded [62], and some dry lake beds that had desertified became lakes again [63]. The soil moisture in the region continued to increase [64], and the annual average precipitation and seasonal average precipitation in the region showed an increasing trend [65]. These environmental events all reflect the evidence of increasing precipitation in northwest China.

Although the Westerly circulation from the ocean (Atlantic) and land seas (Mediterranean, Black Sea, Caspian Sea, etc.) is the main source of water vapor in northwest China, the mechanism that cause increased precipitation in the region is relatively complex. It may not only be a partial response to global warming, but maybe also be related to the Siberian high and the Arctic Oscillation (AO), as well as the latitudinal oscillation of the Westerly jet and the northward movement of the subtropical high belt [65]. However, the essence of the above reasons is that they can promote the enhancement of the Westerly circulation and cause warming and humidification in the northwest China.

However, in addition to the strengthening of the Westerly circulation, the humidification of northwest China may also be affected by the weakening of the EASM.

Some studies have found that the increase of precipitation in the northwest China in recent years is partly related to the weakening of the EASM [62]. According to the reanalysis data of precipitation days, studies have revealed that, in addition to the North Atlantic water vapor transported by the Westerlies, the water vapor of northwest China may also be transported from the tropical Indian Ocean (SASM) and the South China Sea monsoon (EASM) under extreme climatic conditions [62][66].

When the EASM weakens, it is conducive to the westward movement of the western Pacific subtropical high (WPSH) and the increase of Mongolian anticyclone activity [67]. The westward extension of the WPSH promotes the westward transport of water vapor from the eastern Pacific and northern Indian Oceans in summer. The increase of Mongolian anticyclones leads to continuous easterly winds in northern China, which can travel along the northern QTP to the western Tarim Basin in Xinjiang [67]. The two jointly promote the water vapor transport of

the monsoon system from the tropical Indian Ocean and the South China Sea along the eastern and northern QTP into the lower troposphere water vapor in northwest China, as well as from the tropical Indian Ocean into the middle and upper troposphere water vapor in northwest China [67].

In fact, on 30 July 2018, the Wensu rainstorm that caused serious loss of life and property in Aksu, Xinjiang, and the Hami rainstorm on the next day (31 July) were formed under this circulation system [62]. It can be seen that some extreme rainfall phenomena in northwest China are closely related to the extreme westward extension of the subtropical high pressure caused by the weakening of the EASM.

The eastern and western parts of northwest China have different responses to the Westerly and ASM circulations. Although both the strengthening of the Westerly circulation and the weakening of the ASM lead to humidification in northwest China, the latter's impact only occurs under extreme precipitation conditions, rather than conventional effects. However, the extensive area of northwest China, especially its eastern part, is subject to both the conventional influences of the Westerly and ASM as it crosses the northern boundary line of the ASM [68]. Based on the average northern boundary line of the ASM, some studies divided the area of northwest China into two parts: the eastern and western parts (**Figure 6**a). The area east of the boundary line is controlled by the ASM and the area west of the boundary line is controlled by the Westerlies [69].

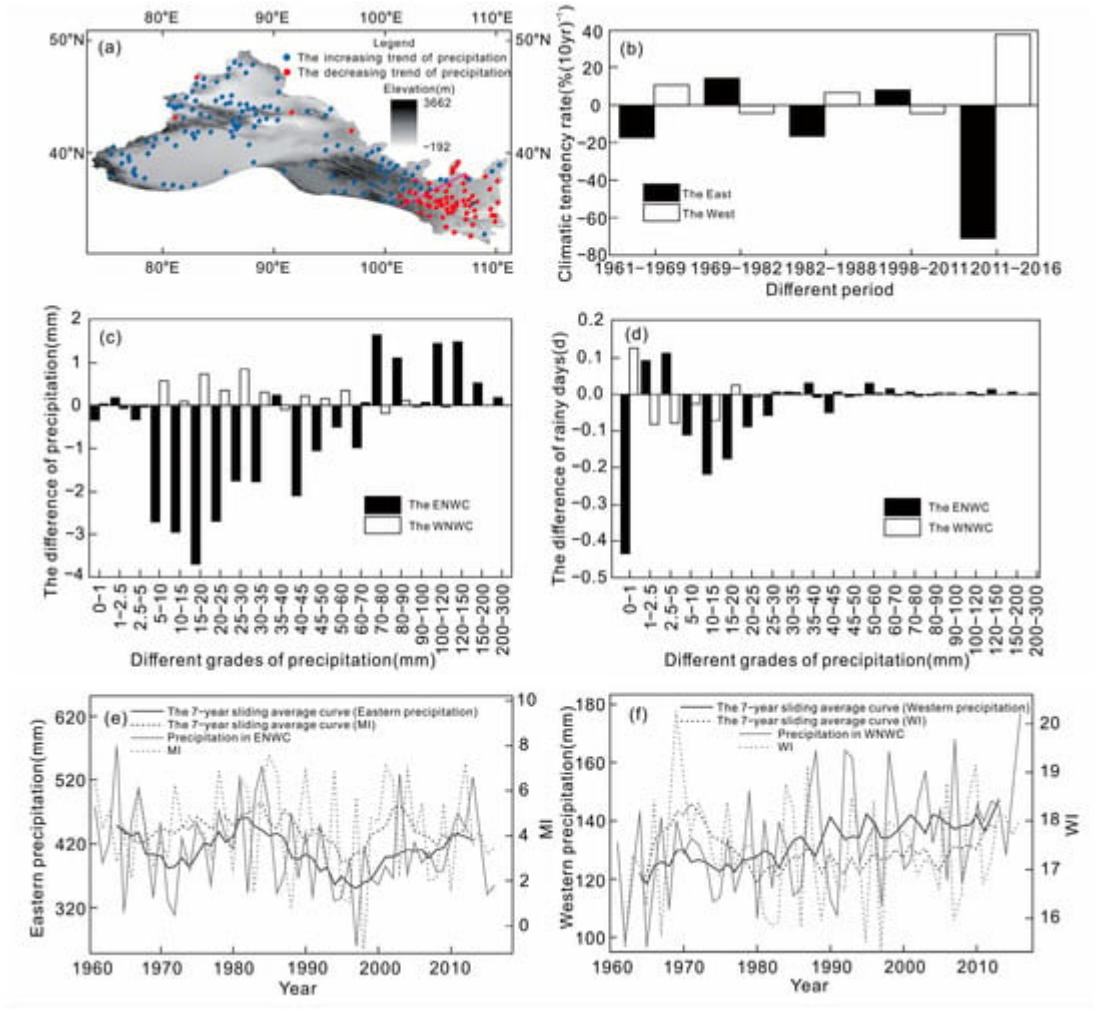

Figure 6. Precipitation seesaw phenomenon in the eastern (ENWC) and western (WNWC) parts of Northwest China (NWC) (modified after [69]). (**a**) Regional division of ENWC and WNWC and the precipitation tendency distribution of stations in the same period. (**b**) The tendency distribution of variation of precipitation anomaly percentage in ENWC and WNWC during flood season from 1961 to 2016. The difference distribution of precipitation (**c**) and rainy days (**d**) in ENWC and WNWC under the WA-EH and WH-EA styles (the WA-EH style means precipitation increases in ENWC and decreases in WNWC, while the WH-EA style is the opposite). The comparison of EASM index and precipitation variation in ENWC (**e**) and the comparison of WI and precipitation variation in WNWC (**f**).

Through the analysis of the differences in precipitation variation between the eastern and western parts of northwest China and their interrelationships with the Westerly and ASM, Zhang Q et al. [69] found that the precipitation variations between the eastern and western parts of northwest China exhibit a significant “seesaw” phenomenon in the interannual, decadal, and overall times scales (**Figure 6**a–d). This phenomenon is related to the anti-phase variation between the ASM index and the Westerly circulation index; that is, the precipitation in the eastern part of northwest China is positively correlated with the summer monsoon index, and the precipitation in the western part is positively correlated with the Westerly index (**Figure 6**e,f). This indicates that the strengthening of the ASM will lead to an increase in precipitation in the eastern part of northwest China, while the strengthening of the Westerly circulation will lead to an increase in precipitation in the western part.

It can also be seen that there is an anti-phase variation relationship between the EASM index and the Westerly index (**Figure 6**e,f). It is not only related to the interaction between the EASM and Westerly circulation through the subtropical high, but also to the common but almost opposite effect of the South Asian high on the EASM and Westerly circulations under the influence of the QTP [69].

2.3. Eastern China (Monsoon Zone)

The impact of the ASM on the climate of East Asia is usually that, when the intensity of the ASM from the ocean changes, its water-vapor-carrying capacity also changes, resulting in an increase or decrease of the total precipitation in East Asia [70].

For the world’s largest monsoon system, namely, the ASM, its large-scale precipitation requires not only sufficient water vapor, but also needs to have another condition, that is, the dynamic conditions for water vapor to rise. In this regard, the WPSH (western Pacific subtropical high) and the SAH (South Asian high, also called the Qinghai–Tibet Plateau high, QTPH) play important roles in it [71]. This process is influenced by both local and middle- and high-latitude circulation factors, which result in a complexity in the relationship between the ASM and precipitation in East Asia.

Studies have shown that many factors can affect the intensity variation of the EASM and its corresponding precipitation configuration, such as the changes of sea surface temperature (SST) in different years [72], the WPSH [73], the SAH [74], the blocking high pressure situation in middle to high latitudes and related water vapor transport

[75], etc. In other words, the anomalies of the EASM are usually accompanied by the anomalies of the WPSH and the SAH. The precipitation in the EASM region is influenced by the northward movement of the WPSH, the eastward shift of the SAH center, and the blocking situation in the Ural region. Moreover, these impacts are not static, but the combination of different factors brings different effects.

In order to better understand the response of precipitation in East Asia to the intensity of the ASM, studies have divided the relationship between monsoon intensity and precipitation into four types [70], namely, the strong monsoon and strong precipitation type, strong monsoon and weak precipitation type, weak monsoon and strong precipitation type, and weak monsoon and weak precipitation type. The strong monsoon and heavy precipitation type often corresponds to the background conditions of a high SST in the North Pacific Ocean, northward movement of the position of the WPSH, and westward movement of the center of the SAH. The strong monsoon and weak precipitation type corresponds to the background conditions of a significantly lower SST in the North Pacific, southward position of the WPSH, and eastward position of the center of the SAH. The weak monsoon and strong precipitation type corresponds to the background conditions of a high SST in the North Pacific, northward position of the WPSH, and westward position of the center of the SAH. The weak monsoon and weak precipitation type corresponds to the background conditions of a low SST in the North Pacific, southward position of the WPSH, and eastward position of the center of the SAH. Therefore, the precipitation in the ASM region will form different types of precipitation under the influence of the ASM and multiple atmospheric systems.

In terms of the interaction between the monsoon and westerly circulations, not only will the changes of the ASM affect the precipitation variation in the northwest of China dominated by the westerly system, but the changes of the Westerly intensity will also affect the precipitation in the ASM region. The impact of the Westerlies on the precipitation in the monsoon region is mainly achieved by affecting the position variation of the subtropical high pressure.

Normally, the strengthening of the Westerlies will “attract” the northward uplift and westward extension of the subtropical high. The area covered by the subtropical high is usually characterized by a prevailing downdraft, sunny weather, and prolonged drought, and its edge area is the convergent and rising area of warm and moist air in the lower layer, which is prone to the formation of thunderstorms and precipitation belts. Therefore, where the subtropical high is located, the central control area of the subtropical high is dry and hot, while the marginal area forms a large amount of monsoon precipitation. In this context, changes in the position of subtropical high pressure will lead to different water-and-heat-combination characteristics in the south and north of the ASM region.

3. Dynamic Mechanism and Influencing Factors of Changes in Monsoon and Westerly Circulations

3.1. Orbital Time Scale

On the orbital time scale of the glacial/interglacial cycles, the climate and environmental change patterns in northwest China dominated by the westerlies is consistent with that of eastern China dominated by the monsoons

[76], showing glacial-to-interglacial-to-glacial cyclical changes. A comparative study on the paleoenvironments between the Chashmanigar loess in Tajikistan bordering northwest China (Westerly region) and the Lingtai loess in the central Loess Plateau of China (monsoon region) has found that not only do they exhibit obvious alternation of loess layers and paleosol layers, but the loess and paleosol layers in both places also have a good consistency in age [17][77], which accords with the Earth's orbital changes in the cycles of glacial and interglacial periods.

In terms of genesis, it is well known that the environmental conditions for the formation of loess and paleosols are different. The loess layer is mainly formed during the cold and dry glacial period, while the paleosol layer is often formed during the warm and humid interglacial period [78][79]. Although the sedimentary rhythms of the Lingtai loess profile in China and the Chashmanigar loess profile in Tajikistan are consistent and the climatic conditions for the formation of loess and paleosol are similar, the atmospheric circulations (wind systems) of the two are fundamentally different.

In the Tajikistan area dominated by the Westerlies, the climate of the loess layer formation was dry, windy, and cold with a high dust content in the atmosphere. The transport and deposition of loess dust were influenced by the Westerlies throughout the year and the Siberian north wind in winter. The climate of the paleosol layer formation in this region was relatively wet, warm, and windy. It was not only affected by the warm temperature during the interglacial period, but also had a richer water vapor content compared to the loess formation period, and the main source of water vapor was the Westerly circulation. It carries a large amount of water vapor from the North Atlantic region and promotes the formation of ancient soil layers in Tajikistan [17][77].

In the Loess Plateau of China under the control of the ASM, the loess layers were formed during the cold and dry glacial period and were mainly influenced by the Siberian northwest wind (winter monsoon). The climate for the formation of the paleosol layers was relatively warm and humid, which is not only related to the global warm climate in the interglacial period, but also related to the large amount of water vapor brought by the strong ASM from the ocean, and the combined effect of the two promoted the formation of the local paleosol [17][77][78][79].

Tajikistan and China, two regions controlled by different atmospheric circulation systems, have formed relatively consistent profiles of loess and paleosol cycles, indicating that, on the orbital time scale of glacial–interglacial cycles, the Westerly circulation that promotes the formation of paleosols in Central Asia and the ASM circulation that promotes the formation of paleosols in the Loess Plateau exhibit consistent intensity changes on this time scale, which proves that the two have an in-phase relationship.

Therefore, the Westerly circulation and the ASM circulation both respond to the changes in solar radiation in the NH on the glacial–interglacial scale and the precession time scale of 20,000 years, and they have an in-phase relationship on the Earth's orbital time scale.

3.2. Suborbital Time Scale

On the suborbital time scale, comprehensive comparisons of various paleoenvironmental records have shown that the changes of solar radiation and SST at high latitudes in the NH may be important factors influencing the

paleoenvironmental changes in the arid Central Asia (ACA) since the Holocene (**Figure 7**). Moreover, these factors may also have significant impacts on the variation of the monsoon circulation intensity in the mid-latitudes [38]. Under the influence of multiple factors, the climate and environmental changes in the Westerly and monsoon regions may be asynchronous on the suborbital time scale (that is, exhibiting an out-of-phase relationship). This was observed during the relatively warm Last Interglacial and Holocene periods.

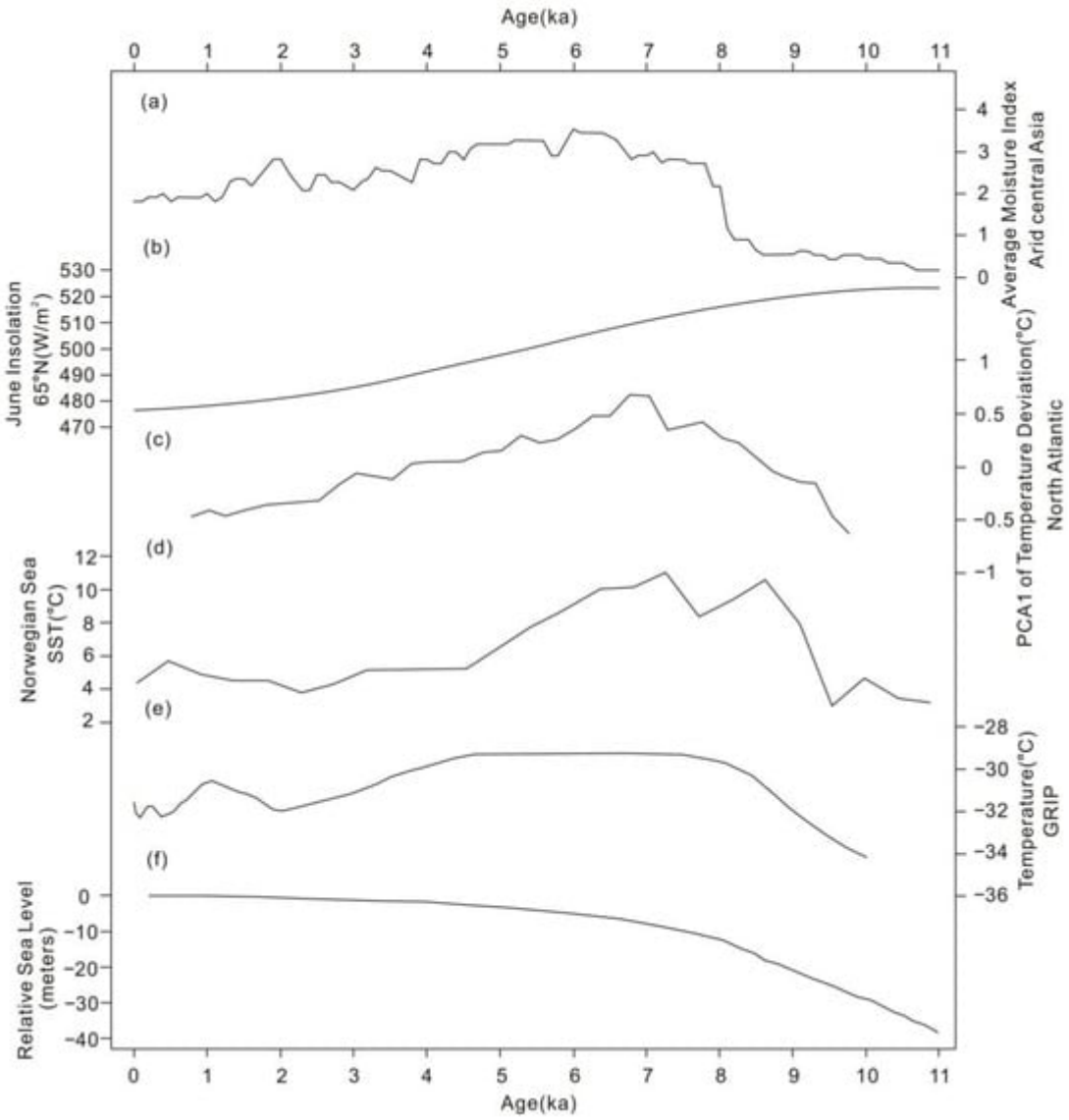

Figure 7. A comprehensive comparison of the Westerlies with multiple global environmental records at the Holocene suborbital scale (cited from [38]). (**a**) Synthesized Holocene mean moisture index in arid Central Asia (ACA); (**b**) correlation with Northern Hemisphere summer insolation [52]; (**c**) sea surface temperature (SST) of the North Atlantic region [80]; (**d**) SST of the Norwegian Sea [81]; (**e**) air temperature from GRIP ice-core [82]; and (**f**) relative sea-level change from Barbados [83].

The loess profiles from the Yili Basin in the Westerly region and the Loess Plateau in the monsoon region both show that, during the Last Interglacial period, the variation of humidity in northwest China lagged behind that in the monsoon region by about 3–5 ka [26]. This reveals that the atmospheric circulation systems that caused the

humidity changes in the two regions were not synchronized during this period. During the Holocene period, as discussed above, the climate and environmental changes in the arid Central Asia and the ASM regions were also asynchronous (**Figure 4**). Environmental changes in the arid region of northwest China are characterized by the early Holocene drought, the middle Holocene humidity, and the late Holocene moderate humidity, while the ASM region exhibits the early Holocene humidity, the middle Holocene relative humidity, and the late Holocene relative drought [38]. This indicates that the Westerly circulation and the ASM circulation exhibit an out-of-phase relationship on the suborbital time scale within the interglacial period.

The reasons for the asynchronous (out-of-phase) evolution of the Westerlies and monsoons at the suborbital scale can be explored by taking the changes of solar radiation and SST during the Holocene as examples.

In the early Holocene, the rise in global temperature and the increase in solar radiation (**Figure 4**) led to an increase of the sea–land temperature gradient and evaporation in East Asia, and the intensity of the ASM was enhanced and a large amount of water vapor was carried from the ocean to East Asia [44]. Therefore, the climatic environment of the ASM region was relatively humid in the early Holocene. However, for the northwest region of China at the middle latitudes, the strong solar radiation in summer in the early Holocene would lead to intense local evaporation. At the same time, due to the significant melting of the ice sheet in Greenland, the sea water temperature in the North Atlantic Ocean was lower and the sea surface evaporation was reduced, so the water vapor content brought by the Westerly circulation decreased, leading to a dry climate in northwest China (**Figure 8**). In winter, the increase of solar radiation also leads to an increase of SST in the north Atlantic Ocean, a decrease of meridional temperature gradient, a decrease of the Westerly intensity, a decrease of evaporation due to the lower winter temperature, and a decrease of water vapor content brought by the Westerlies, leading to further drought in northwest China [41].

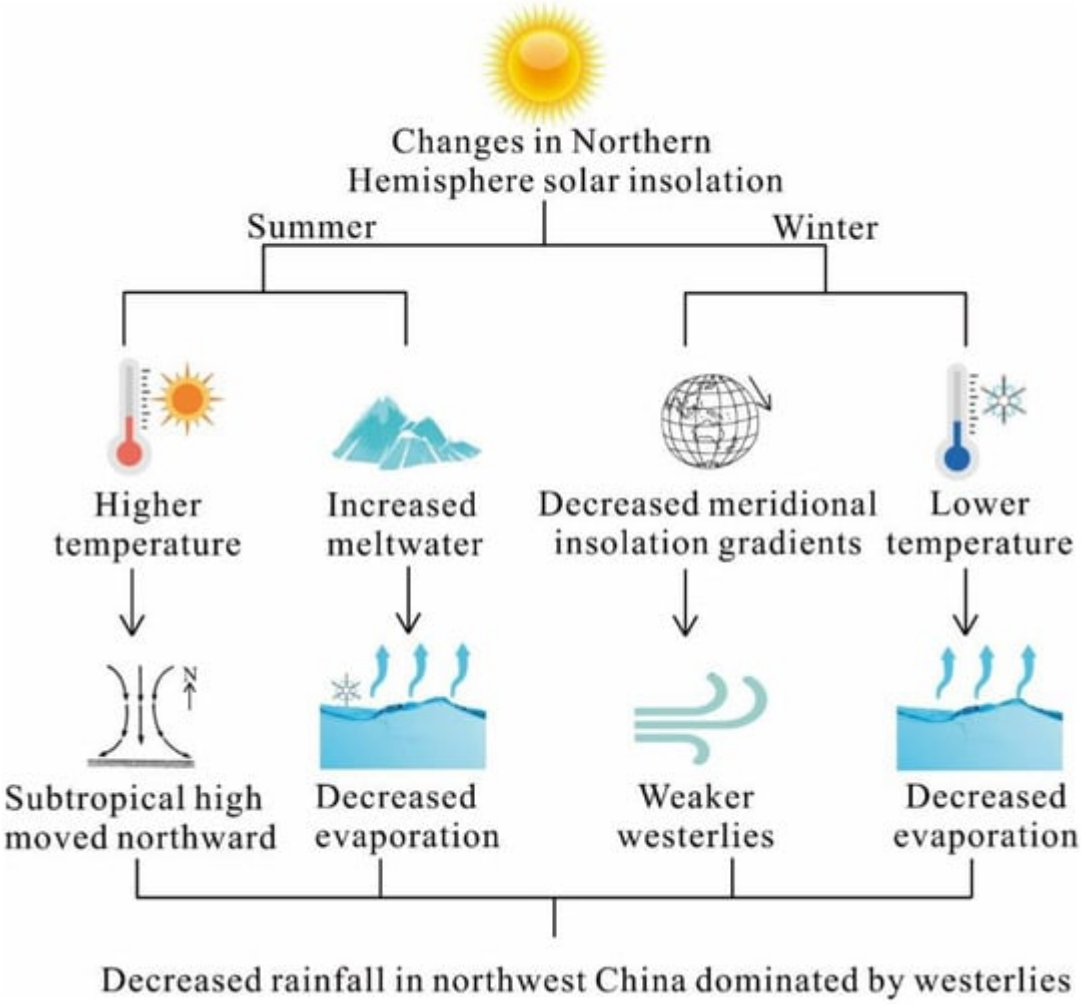

Figure 8. Changes in solar radiation in the early Holocene in the NH led to climatic drought in the Westerly region [76].

After the middle Holocene, the solar radiation in the NH was slightly weaker than in the earlier period but still relatively strong (**Figure 7**). Due to the relative decrease in solar radiation, the ASM also showed a weakening trend in the middle Holocene [44], but the climate in the monsoon region was still relatively humid at this time, with only a decrease in the degree of humidity compared to the early Holocene (**Figure 4**). For the Westerly region during this period, because the ice sheet in the NH gradually decreases but the SST in the North Atlantic began to rise, the water vapor content of the Westerly circulation increased and the activity of low-level cyclones increased, resulting in a large increase in the wetness of northwest China. Therefore, under the influence of a high SST in the North Atlantic and high temperature in the middle latitudes, the enhanced water vapor transport of the Westerly circulation and increased cyclone activity in the region led to a higher degree of humidity in northwest China during this period [76].

In summary, the ASM was mainly controlled by the amount of summer solar radiation since the Holocene [54]; coupled with the changes of SST and regional surface processes, these factors collectively contributed to the key driven mechanism that caused the environmental changes in the Westerly and ASM regions to show they were out-of-phase at the suborbital scale during the Holocene [41].

3.3. Millennial to Centennial Time Scale

Multiple paleoenvironmental records and modeling studies have shown that the weakening of the North Atlantic overturning circulation (AMOC) and the expansion of ice volume in the NH since the penultimate and last glacial periods can lead to rapid climate change in the North Atlantic region on a millennium to centennial time scale (**Figure 9**). At the same time, it affects the intensity and location changes of the Westerly circulation, and then transmits to eastern Asia through the Westerly circulation, causing rapid climate and environmental changes in the SAM region [44][84][85][86][87].

Abrupt climate change events on the millennium time scale that occurred during the LGP (such as the Heinrich and DO events) were largely associated with the weakening of the AMOC [88][89]. The link between rapid cold events in the North Atlantic Ocean and weak ASM on a centennial to millennium time scale since the LGP has also been confirmed by various climatic records (**Figure 9**). For example, during the Younger Dryas (YD) event and 9.5–8.5 ka B.P., the EASM precipitation on the millennium time scale showed a significant weakening, which corresponded to the weakening of the AMOC [90][91].

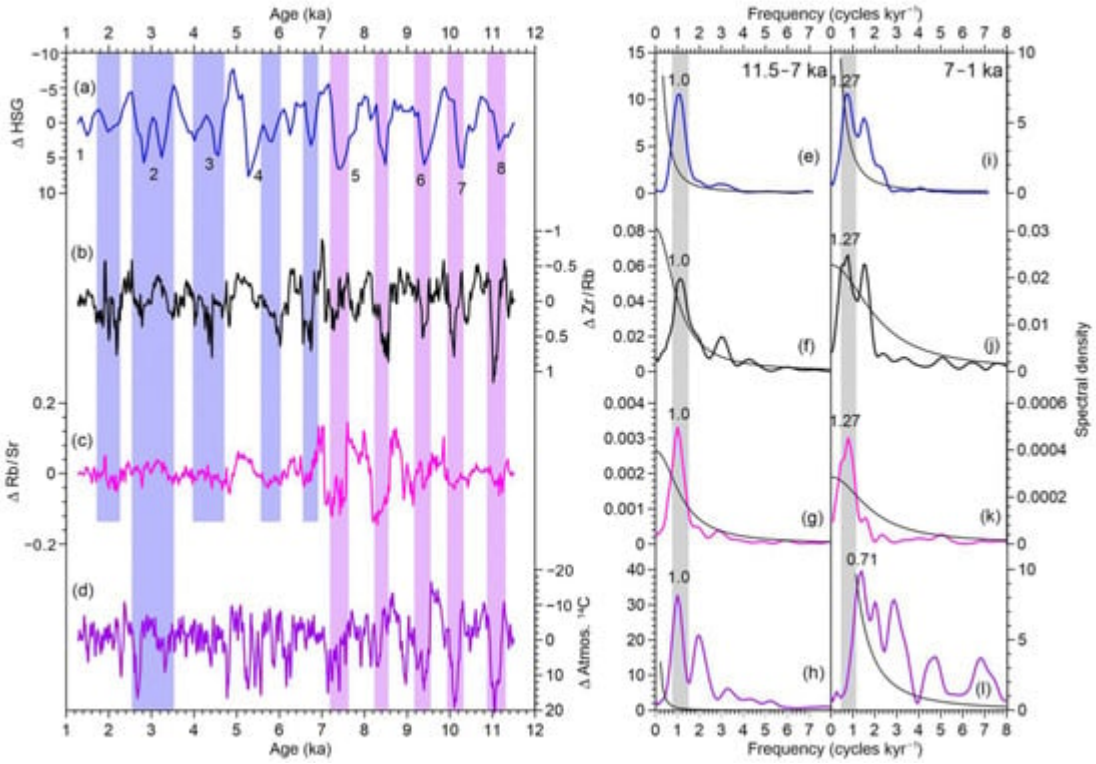

Figure 9. A comparison between the records of the Asian summer monsoon and North Atlantic abrupt events (cited from [91]). (**a**–**d**) Centennial components of (**b**) Zr/Rb and (**c**) Rb/Sr with (**a**) the North Atlantic HSG [92] and (**d**) atmosphere 14C record [93]. The purple and blue bars indicate abrupt monsoon events. The numbers 1–8 in figure (**a**) indicate the selected event cycles which are used for the spectral analyses of periodicity in figure (**e**–**l**). Plots (**e**–**l**) show the spectra of the proxy records during the (**e**–**h**) Early and (**i**–**l**) Late Holocene [91]. Spectral peaks that

are above the 80% confidence levels (black lines) are marked. The grey vertical bands indicate the most significant cycle [91].

References

1. Rea, D.K.; Snoeckx, H.; Joseph, L.H. Late Cenozoic Eolian deposition in the North Pacific: Asian drying, Tibetan uplift, and cooling of the northern hemisphere. Paleoceanography 1998, 13, 215–224.
2. Liu, D.; Zheng, M.; Guo, Z. Initiation and evolution of the Asian monsoon system timely coupled with the ice-sheet growth and the tectonic movements in Asia. Quat. Sci. 1998, 18, 194–204.
3. Wu, F.; Fang, X.; Yang, Y.; Dupont-Nivet, G.; Nie, J.; Fluteau, F.; Zhang, T.; Han, W. Reorganization of Asian climate in relation to Tibetan Plateau uplift. Nat. Rev. Earth Environ. 2022, 3, 684–700.
4. Shi, Y.; Tang, M. Discussion on the relationship between the second stage uplift of the Qinghai Tibet Plateau and the development of the Asian monsoon. Sci. China (Ser. D) 1998, 28, 263–271.
5. Cao, J.; Zhang, X.; Cheng, Y.; Lu, H. Size distribution of the late Cenozoic red clay and the winter monsoon variations. Mar. Geol. Quat. Geol. 2001, 21, 99–106.
6. Guo, Z. The Evolution History of the Monsoon Recorded by the 22-8 Ma Wind Dust Deposition See: Ding Zhongli et al. Research on the Integration of Environmental Evolution in Western China; Meteorological Publishing House: Beijing, China, 2010.
7. An, Z. The history and variability of East Asian monsoon climate. Chin. Sci. Bull. 2000, 45, 238–249.
8. Sun, D.; Shaw, J.; An, Z.; Cheng, M.; Yue, L. Magnetostratigraphy and paleoclimatic interpretation of a continuous 7.2 Ma late Cenozoic eolian sediments from the Chinese Loess Plateau. Geophys. Res. Lett. 1998, 25, 85–88.
9. Liu, X. Influences of Qinghai-Xizang (Tibet) Plateau uplift on the atmospheric circulation, global climate and environment changes. Plateau Meteorol. 1999, 18, 321–332.
10. Wu, G.; Pan, B.; Guan, Q.; Gao, H. Reviews of studies on the Mid-Pleistocene climatic transition and 100 ka cycle. Adv. Earth Sci. 2002, 17, 605–611.
11. Wang, T.; Sun, Y.; Liu, X. Mid-Pleistocene climate transition: Characteristic, mechanism and perspective. Chin. Sci. Bull. 2017, 62, 3861–3872.
12. Wang, F.; Li, Z.; Sun, X.; Li, B.; Wang, X.; Chen, F. A 1200 ka stable isotope record from the center of the Badain Jaran Desert, northwestern China: Implications for the variation and interplay

of the westerlies and the Asian summer monsoon. Geochem. Geophys. Geosyst. 2021, 22, e2020GC009575.

13. Han, W.; Fang, X.; Ye, C.; Teng, X.; Zhang, T. Tibet forcing Quaternary stepwise enhancement of westerly jet and Central Asian aridification: Carbonate isotope records from deep drilling in the Qaidam salt playa, NE Tibet. Glob. Planet. Chang. 2014, 116, 68–75.
14. Fang, X.; Lv, L.; Yang, S.; Li, J.; An, Z.; Jiang, P.; Chen, X. Loess in Kunlun Mountains and its implications on desert development and Tibetan Plateau uplift in West China. Sci. China Ser. D-Earth Sci. 2002, 45, 289–299.
15. Fang, X.; Shi, Z.; Yang, S.; Yan, M.; Li, J.; Jiang, P. Loess in the Tian Shan and its implications for the development of the Gurbantunggut Desert and drying of northern Xinjiang. Chin. Sci. Bull. 2002, 47, 1381–1387.
16. An, Z.; Huang, Y.; Liu, W.; Guo, Z.; Clemens, S.; Li, L.; Prell, W.; Ning, Y.; Cai, Y.; Zhou, W.; et al. Multiple expansions of C4 plant biomass in East Asia since 7 Ma coupled with strengthened monsoon circulation. Geology 2005, 33, 705–708.
17. Ding, Z.; Ranov, V.; Yang, S.; Finaev, A.; Han, J.; Wang, G. The loess record in southern Tajikistan and correlation with Chinese loess. Earth Planet. Sci. Lett. 2002, 200, 387–400.
18. Li, J.; Fang, X. Uplift of the Tibetan Plateau and environmental changes. Chin. Sci. Bull. 1999, 44, 2117–2124.
19. Lv, Y.; Zhang, C.; Fu, Y.; Wu, H.; Hao, Q.; Qiao, Y.; Guo, Z. Clay mineralogical and geochemical record from a loess-paleosol sequence in Chinese Loess Plateau during the past 880 ka and the implication on the East Asian Summer Monsoon. Quat. Sci. 2022, 42, 921–938.
20. Huang, C.; Pang, J.; Huang, P.; Hou, C.; Han, Y. High-resolution studies of the oldest cultivated soils in the southern Loess Plateau of China. Catena 2002, 47, 29–42.
21. Huang, C.; Pang, J.; Chen, S.; Zhang, Z. Holocene dust accumulation and the formation of polycyclic cinnamon soils (luvisols) in the Chinese Loess Plateau. Earth Surf. Process. Landf. 2003, 28, 1259–1270.
22. Chen, C.; Lan, H.; Lou, J.; Chen, Y. The dry Holocene megathermal in inner Mongolia. Palaeogeogr. Palaeoclimatol. Palaeoecol. 2003, 193, 181–200.
23. Pye, K.; Zhou, L. Late Pleistocene and Holocene aeolian dust deposition in North China and the Northwest Pacific Ocean. Palaeogeogr. Palaeoclimatol. Palaeoecol. 1989, 73, 11–23.
24. Linsley, B.K. Oxygen-isotope record of sea level and climate variations in the Sulu Sea over the past 150,000 years. Nature 1996, 380, 234–237.
25. Jia, J.; Xia, D.; Wang, Y.; Wang, B.; Lu, H.; Zhao, S. East Asian monsoon evolution during the Eemian, as recorded in the western Chinese Loess Plateau. Quat. Int. 2016, 399, 156–164.

26. Jia, J.; Gao, F.; Xia, D.; Huang, W.; Chen, F. Moisture variations in arid Central Asia and its out-of-phase relationship with the Asian Monsoon during MIS 5: Evidence from loess records. J. Quat. Sci. 2018, 33, 435–443.
27. Chen, F.; Jia, J.; Chen, J.; Li, G.; Zhang, X.; Xie, H.; Xia, D.; Huang, W.; An, C. A persistent Holocene wetting trend in arid Central Asia, with wettest conditions in the late Holocene, revealed by multi-proxy analyses of loess-paleosol sequences in Xinjiang, China. Quat. Sci. Rev. 2016, 146, 134–146.
28. Dansgaard, W. North Atlantic climatic oscillations revealed by deep Greenland ice cores. Clim. Process. Clim. Sensit. 1984, 29, 288–298.
29. Heinrich, H. Origin and consequences of cyclic ice rafting in the Northeast Atlantic Ocean during the past 130,000 years. Quat. Res. 1988, 29, 142–152.
30. Song, Y.; Zeng, M.; Chen, X.; Li, Y.; Chang, H.; An, Z.; Guo, X. Abrupt climatic events recorded by the Ili loess during the last glaciation in Central Asia: Evidence from grain-size and minerals. J. Asian Earth Sci. 2018, 155, 58–67.
31. Rao, Z.; Chen, F.; Cheng, H.; Liu, W.; Wang, G.; Lai, Z.; Bloemendal, J. High-resolution summer precipitation variations in the western Chinese Loess Plateau during the last glacial. Sci. Rep. 2013, 3, 2785.
32. Cheng, H.; Edwards, R.L.; Sinha, A.; Sptl, C.; Yi, L.; Chen, S.; Kelly, M.; Kathayat, G.; Wang, X.; Li, X.; et al. The Asian monsoon over the past 640,000 years and ice age terminations. Nature 2016, 534, 640–646.
33. Wang, Y.; Cheng, H.; Edwards, R.L.; An, Z.; Wu, J.; Shen, C.; Dorale, J.A. A high-resolution absolute-dated late Pleistocene monsoon record from Hulu Cave, China. Science 2001, 294, 2345–2348.
34. Chen, J.; An, Z.; Wang, Y.; Ji, J.; Chen, Y.; Lu, H. Rb/Sr distribution and paleomonsoon changes in the recent 800ka Luochuan loess profile. Sci. China (Ser. D) 1998, 28, 498–504.
35. Andersen, K.K.; Azuma, N.; Barnola, J.M.; Bigler, M.; Biscaye, P.; Caillon, N.; Chappellaz, J.; Clausen, H.B.; Dahljensen, D.; Fischer, H.; et al. High-resolution record of northern hemisphere climate extending into the last interglacial period. Nature 2004, 431, 147–151.
36. Chen, F.; Chen, J.; Huang, W. A discussion on the westerly-dominated climate model in mid-latitude Asia during the modern interglacial period. Earth Sci. Front. 2009, 16, 23–32.
37. Jin, L.; Chen, F.; Morrill, C.; Otto-Bliesner, B.L.; Rosenbloom, N. Causes of early Holocene desertification in arid Central Asia. Clim. Dyn. 2012, 38, 1577–1591.
38. Chen, F.; Yu, Z.; Yang, M.; Ito, E.; Wang, S.; Madsen, D.B.; Huang, X.; Zhao, Y.; Sato, T.; Birks, H.J.B.; et al. Holocene moisture evolution in arid Central Asia and its out-of-phase relationship

with Asian monsoon history. Quat. Sci. Rev. 2008, 27, 351–364.

39. Chen, F.; Xu, Q.; Chen, J.; Birks, H.J.B.; Liu, J.; Zhang, S.; Jin, L.; An, C.; Telford, R.J.; Cao, X.; et al. East Asian summer monsoon precipitation variability since the last deglaciation. Sci. Rep. 2015, 5, 11186.
40. Herzschuh, U. Palaeo-moisture evolution in monsoonal Central Asia during the last 50,000 years. Quat. Sci. Rev. 2006, 25, 163–178.
41. Zhang, X.; Jin, L.; Huang, W.; Chen, F. Forcing mechanisms of orbital-scale changes in winter rainfall over northwestern China during the Holocene. Holocene 2016, 26, 549–555.
42. Yuan, D.; Cheng, H.; Edwards, R.L.; Dykoski, C.A.; Kelly, M.J.; Zhang, M.; Qing, J.; Lin, Y.; Wang, Y.; Wu, J.; et al. Timing, duration, and transitions of the Last Interglacial Asian monsoon. Science 2004, 304, 575–578.
43. Zhang, P.; Cheng, H.; Edwards, R.L.; Chen, F.; Wang, Y.; Yang, X.; Liu, J.; Tan, M.; Wang, X.; Liu, J.; et al. A test of climate, sun, and culture relationships from an 1810-Year Chinese cave record. Science 2008, 322, 940–942.
44. Wang, Y.; Cheng, H.; Edwards, R.L.; He, Y.; Kong, X.; An, Z.; Wu, J.; Kelly, M.J.; Dykoski, C.A.; Li, X. The Holocene Asian monsoon: Links to solar changes and North Atlantic climate. Science 2005, 308, 854–857.
45. Shao, X.; Wang, Y.; Cheng, H.; Kong, X.; Wu, J. Long-term trend and abrupt events of the Holocene Asian monsoon inferred from a stalagmite d18O record from Shennongjia in Central China. Chin. Sci. Bull. 2006, 51, 221–228.
46. Fleitmann, D.; Burns, S.J.; Mudelsee, M.; Neff, U.; Kramers, J.; Mangini, A.; Matter, A. Holocene Forcing of the Indian Monsoon recorded in a stalagmite from Southern Oman. Science 2003, 300, 1737–1739.
47. Hong, Y.; Hong, B.; Lin, Q.; Zhu, Y.; Shibata, Y.; Hirota, M.; Uchida, M.; Leng, X.; Jiang, H.; Xu, H.; et al. Correlation between Indian Ocean summer monsoon and North Atlantic climate during the Holocene. Earth Planet. Sci. Lett. 2003, 211, 371–380.
48. Hong, Y.; Hhong, B.; Lin, Q.; Shibata, Y.; Hirota, M.; Zhu, Y.; Leng, X.; Wang, Y.; Wang, H.; Yi, L. Inverse phase oscillations between the East Asian and Indian Ocean summer monsoons during the last 12000 years and paleo-El Nio. Earth Planet. Sci. Lett. 2005, 231, 337–346.
49. Gu, Z.; Liu, J.; Yuan, B.; Liu, D.; Liu, R.; Liu, Y.; Yaskawa, K. Monsoon variations of the Qinghai-Xizang Plateau during the last 12,000 years—Geochemical evidence from the sediments in the Siling Lake. Chin. Sci. Bull. 1993, 38, 577–581.
50. Liu, X.; Shen, J.; Wang, S.; Wang, Y.; Liu, W. Southwest monsoon changes indicated by oxygen isotope of ostracode shells from sediments in Qinghai Lake since the Lateglacial. Chin. Sci. Bull.

2007, 52, 539–544.

51. Gupta, A.K.; Anderson, D.M.; Overpeck, J.T. Abrupt changes in the Asian southwest monsoon during the Holocene and their links to the North Atlantic Ocean. Nature 2003, 421, 354–357.
52. Berger, A.; Loutre, M.F. Insolation values for the climate of the last 10,000,000 years. Quat. Sci. Rev. 1991, 10, 297–317.
53. Chen, F.; Huang, X.; Zhang, J.; Holmes, J.A.; Chen, J. Humid Little Ice Age in and Central Asia documented by Bosten Lake, Xinjiang, China. Sci. China Ser. D-Earth Sci. 2006, 49, 1280–1290.
54. Jin, L.; Schneider, B.; Park, W.; Latif, M.; Khon, V.; Zhang, X. The spatial-temporal patterns of Asian summer monsoon precipitation in response to Holocene insolation change: A model-data synthesis. Quat. Sci. Rev. 2014, 85, 47–62.
55. An, Z.; Porter, S.C.; Kutzbach, J.E.; Wu, X.; Wang, S.; Liu, X.; Li, X.; Zhou, W. Asynchronous Holocene optimum of the East Asian monsoon. Quat. Sci. Rev. 2000, 19, 743–762.
56. Yao, T.; Park, S.; Shen, M.; Gao, J.; Yang, W.; Zhang, G.; Lei, Y.; Gao, Y.; Zhu, L.; Xu, B.; et al. Chained impacts on modern environment of interaction between westerlies and Indian monsoon on Tibetan Plateau. Bull. Chin. Acad. Sci. 2017, 32, 976–984.
57. Chen, B.; Xu, X.; Yang, S.; Zhang, W. On the origin and destination of atmospheric moisture and air mass over the Tibetan Plateau. Theor. Appl. Climatol. 2012, 110, 423–435.
58. Zhou, T.; Gao, J.; Zhao, Y.; Zhang, L.; Zhang, W. Water vapor transport processes on Asian water tower. Bull. Chin. Acad. Sci. 2019, 34, 1210–1219.
59. Duan, K.; Yao, T.; Wang, N.; Tian, L.; Xu, B. The difference in precipitation variability between the north and south Tibetan Plateaus. J. Glaciol. Geocryol. 2008, 30, 726–732.
60. Yao, T.; Masson-Delmotte, V.; Gao, J.; Yu, W.; Yang, X.; Risi, C.; Sturm, C.; Werner, M.; Zhao, H.; He, Y. A review of climatic controls δ18O in precipitation over the Tibetan Plateau: Observations and simulations. Rev. Geophys. 2013, 51, 525–548.
61. Guo, L.; Zhu, C. Coupling mode of westerly–monsoonal flow over the Tibetan Plateau and its seasonal variation. Chin. J. Atmos. Sci. 2022, 46, 1017–1029.
62. Chen, C.; Zhang, X.; Lu, H.; Jin, L.; Du, Y.; Chen, F. Increasing summer precipitation in arid Central Asia linked to the weakening of the East Asian summer monsoon in the recent decades. Int. J. Climatol. 2021, 41, 1024–1038.
63. Hu, R.; Jiang, F.; Wang, Y.; Fan, Z. A study on signals and effects of climatic pattern change from warm-dry to warm-wet in Xinjiang. Arid Land Geogr. 2002, 25, 194–200.
64. Li, J.; Gou, X.; Cook, E.R.; Chen, F. Tree-ring based drought reconstruction for the Central Tien Shan area in northwest China. Geophys. Res. Lett. 2006, 33, L07715.

65. Chen, F.; Huang, W.; Jin, L.; Chen, J.; Wang, J. Spatiotemporal precipitation variations in the arid Central Asia in the context of global warming. Sci. China Earth Sci. 2011, 41, 1647–1657.
66. Chen, F.; Chen, J.; Huang, W. Weakened East Asian summer monsoon triggers increased precipitation in Northwest China. Sci. China Earth Sci. 2021, 64, 835–837.
67. Huang, W.; Feng, S.; Chen, J.; Chen, F. Physical Mechanisms of summer precipitation variations in the Tarim Basin in northwestern China. J. Clim. 2015, 28, 3579–3591.
68. Chen, J.; Huang, W.; Jin, L.; Chen, J.; Chen, S. A climatological northern boundry index for the East Asian summer and its interannual variability. Sci. China Earth Sci. 2018, 61, 13–22.
69. Zhang, Q.; Lin, J.; Liu, W.; Han, L. Precipitation seesaw phenomenon and its formation mechanism in the eastern and western parts of Northwest China during the flood season. Sci. China Earth Sci. 2019, 62, 2083–2098.
70. Liu, C.; Wang, H.; Jiang, D. The configurable relationships between summer monsoon and precipitation over East Asia. Chin. J. Atmos. Sci. 2004, 28, 699–712.
71. Guo, Q. The variations of summer monsoon in East Asia and the rainfall over China. J. Trop. Meteorol. 1985, 1, 44–52.
72. Huang, X.; Xu, H.; Deng, J. Long-term rising of SST over the marginal seas of China in winter and its impact on precipitation in China. Acta Meteorol. Sin. 2015, 73, 505–514.
73. Yu, Y.; Wang, S.; Qian, Z.; Song, M.; Wang, A. Climatic linkages between SHWP position and EASM rainy-belts and areas in east part of China in summer half year. Plateau Meteorol. 2013, 32, 1510–1525.
74. Zhang, Y.; Li, Y.; Wei, L.; Liu, K. Effects of south Asia high and western Pacific subtropical high on the summer precipitation anomalies over southwest China. J. Arid Meteorol. 2013, 31, 464–470.
75. Zhang, Q.; Tao, S. Influence of Asian mid-high latitude circulation on East Asian summer rainfall. Acta Meteorol. Sinia 1998, 56, 199–211.
76. Chen, F.; Chen, J.; Huang, W.; Chen, S.; Huang, X.; Jin, L.; Jia, J.; Zhang, X.; An, C.; Zhang, J.; et al. Westerlies Asia and monsoonal Asia: Spatiotemporal differences in climate change and possible mechanisms on decadal to sub-orbital timescales. Earth-Sci. Rev. 2019, 192, 337–354.
77. Yang, S.; Ding, F.; Ding, Z. Pleistocene chemical weathering history of Asian arid and semi-arid regions recorded in loess deposits of China and Tajikistan. Geochim. Cosmochim. Acta 2006, 70, 1695–1709.
78. Liu, T. Loess and the Environment; China Ocean Press: Beijing, China, 1985.
79. Lu, H.; An, Z. The paleoclimatic significance of grain size composition of Loess Plateau. Sci. China (Ser. D) 1998, 28, 278–283.

80. Kaplan, M.R.; Wolfe, A.P. Spatial and temporal variability of Holocene temperature in the North Atlantic region. Quat. Res. 2006, 65, 223–231.
81. Koc, N.; Jansen, E.; Haflidason, H. Paleoceanographic reconstructions of surface ocean conditions in the Greenland, Iceland and Norwegian Seas through the last 14 ka based on diatoms. Quat. Sci. Rev. 1993, 12, 115–140.
82. Dahl-Jensen, D.; Mosegaard, K.; Gundestrup, N.; Clow, G.D.; Johnsen, S.J.; Hansen, A.W.; Balling, N. Past temperatures directly from the Greenland ice sheet. Science 1998, 282, 268–271.
83. Peltier, W.R.; Fairbanks, R.G. Global glacial ice volume and Last Glacial maximum duration from an extended Barbados sea level record. Quat. Sci. Rev. 2006, 25, 3322–3337.
84. Guo, Z.; Liu, T.; Guiot, J.; Wu, N.; Lu, H.; Han, J.; Liu, J.; Gu, Z. High frequency pulses of East Asian monsoon climate in the last two glaciations: Link with the North Atlantic. Clim. Dyn. 1996, 12, 701–709.
85. Yanase, W.; Abe-Ouchi, A. The LGM surface climate and atmospheric circulation over East Asia and the North Pacific in the PMIP2 coupled model simulations. Clim. Past 2007, 3, 439–451.
86. Liu, Y.; Henderson, G.M.; Hu, C.; Mason, A.J.; Charnley, N.; Johnson, K.R.; Xie, S. Links between the East Asian monsoon and North Atlantic climate during the 8200-year event. Nat. Geosci. 2013, 6, 117–120.
87. Porter, S.C.; An, Z.S. Correlation between climate events in the North-Altantic and China during last glaciation. Nature 1995, 375, 305–308.
88. Jin, L.; Chen, F.; Ganopolski, A.; Claussen, M. Response of East Asian climate to Dansgaard/Oeschger and Heinrich events in a coupled model of intermediate complexity. J. Geophys. Res.-Atmos. 2007, 112, D06117.
89. Mcmanus, J.F.; Francois, R.; Gherardi, J.M.; Keigwin, L.D.; Brown-Leger, S. Collapse and rapid resumption of Atlantic meridional circulation linked to deglacial climate changes. Nature 2004, 428, 834–837.
90. Praetorius, S.K.; Mcmanus, J.F.; Oppo, D.W.; Curry, W.B. Episodic reductions in bottom-water currents since the last ice age. Nat. Geosci. 2008, 1, 449–452.
91. Liu, X.; Sun, Y.; Vandenberghe, J.; Cheng, P.; Zhang, X.; Gowan, E.J.; Lohmann, G.; An, Z. Centennial- to millennial-scale monsoon changes since the last deglaciation linked to solar activities and North Atlantic cooling. Clim. Past 2020, 16, 315–324.
92. Bond, G.; Kromer, B.; Beer, J.; Muscheler, R.; Evans, M.N.; Showers, W.; Hoffmann, S.; Lotti-Bond, R.; Hajdas, I.; Bonani, G. Persistent solar influence on North Atlantic climate during the Holocene. Science 2001, 294, 2130–2136.

93. Reimer, P.J.; Bard, E.; Bayliss, A.; Beck, J.W.; Blackwell, P.G.; Ramsey, C.B.; Buck, C.E.; Cheng, H.; Edwards, R.L.; Friedrich, M.; et al. IntCal13 and Marine13 radiocarbon age calibration curves 0–50,000 years cal BP. Radiocarbon 2013, 55, 1869–1887.

Retrieved from https://encyclopedia.pub/entry/history/show/125632